

# DC-DC CONVERTER WITH DUAL ACTIVE-CLAMPING CIRCUIT FOR LOW VOLTAGE PHOTOVOLTAIC SOURCES

B.GAMYA<sup>1</sup>, RAMESH R.HALAKURKI<sup>2</sup>

M.TECH SCHOLAR, DEPT. OF EEE, SITAMS, CHITTOOR, ANDHRA PRADESH, INDIA<sup>1</sup>

PROFESSOR, DEPT. OF EEE, SITAMS, CHITTOOR, ANDHRA PRADESH, INDIA<sup>2</sup>

**Abstract:** This paper proposes a DC-DC converter with dual active clamping circuit for low voltage photovoltaic (PV) dc-dc converter. The proposed dc-dc converter is controlled by asymmetrical pulse width modulation (APWM) technique. The voltage stress of power switches is reduced at low voltage sources. Zero-current turn-off of output diodes is achieved at low-voltage side. power efficiency is improved by reducing the switching power losses A modified proportional and integral controller is also suggested to achieve fast output voltage control. The dynamic response of the proposed converter is improved. The performance of the proposed converter is verified based on an experimental prototype for a 200-W PV module.

**Key Words:** DC-DC converter, soft-switching, zero-current switching (ZCS), photovoltaic (PV), dynamic response.

\*\*\*

## 1. INTRODUCTION

The photovoltaic (PV) module-integrated converter (MIC) System is the key technology for the future distributed production of electricity using solar energy. The PV MIC system offers “plug and play” concept, greatly optimizing the energy yield from the PV module. Each PV module has its own power conversion system, generating the maximum power from the PV module [1]. To make the PV MIC system commercially variable, a low- cost and high-efficiency power conversion scheme should be developed.

The PV module voltage has a low-voltage characteristic. In order to deliver electric power in to the grid, the low PV module voltage should be converted into a high dc-voltage. Thus, a dc-dc converter with high-voltage gain is needed. The active-bridge dc-dc converter has been used for low-voltage PV sources [2]. The power switches at low-voltage side are turned ON at zero voltage. However, the output diode at high-voltage side has high switching power losses due to its reverse-recovery current [3]. The half-bridge dc-dc converter has been presented to reduce switching power losses at high voltage side [4]. The output diodes are turned OFF at zero current by using the voltage doubler rectifier. However, an additional half-wave rectifier is needed, which increases switching power losses. Alternatively, the active-clamped dc-dc converter has been used for low-voltage PV sources [5]. It uses the active-clamping circuit and the resonant voltage doubler rectifier. However, the active clamping circuit increases the voltage stress of power switches at low-voltage side, causing high switching power losses. Additionally, thermal management problems should be considered for a practical design of the PV MIC system.

Considering the dynamic response of the converter, bandwidth limitations of conventional controllers have forced power electronics engineers to increase switching frequency or increase output capacitor [6].such hardware modification results in lower efficiency and higher component cost. However, by improving the controller's dynamic response, the transient performance of the converter can be improved.

Therefore, it is not only necessary but also practical to improve both power efficiency and dynamic response of the dc-dc converter for low-voltage PV sources. This paper proposes a DC-DC converter with dual active clamping circuit for low-voltage PV sources. An improved active-clamped dc-dc converter is presented by using a dual active clamping circuit. The voltage stress of power switches can be reduced at low-voltage side. Also, a modified proportional and integral (PI) controller is suggested for fast output voltage control. The transient performance of the proposed converter is improved. All control functions are implemented in software with a single-chip microcontroller. The proposed converter is realized with minimal hardware with a low cost. The operation of the proposed converter is described. The control strategy is presented, including the fast output voltage control and its digital implementation. The performance of the proposed converter is verified using a 200-W experimental prototype. The experimental results confirm that a high efficiency of 97.5% is achieved at 50-V input voltage for 200-W output power with an improved dynamic performance.

## II. CONVERTER OPERATION

Fig.1.shows the circuit diagram of the proposed dc-dc converter. The converter consists of main Switches ( $S_1, S_4$ ), the dual active-clamping circuit ( $S_2, S_3, C_c$ ), the transformer  $T$ , and the resonant voltage doubler rectifier ( $L_{rk}, C_r, D_{o1}, D_{o2}$ ). The main switches ( $S_1, S_4$ ) and auxiliary switches ( $S_2, S_3$ ) operate complementarily with a short dead time. All switches are the metal-oxide-semiconductor field-effect transistors.

They are considered ideal switches except their body diodes ( $D_{i1} - D_{i4}$ ) and output capacitors ( $C_{i1} - C_{i4}$ ).  $C_i$  is the input capacitor.  $C_c$  is the clamping capacitor.  $C_o$  is the output capacitor. The capacitors  $C_i, C_c$  and  $C_o$  are large enough so that their voltages  $V_i, V_c$  and  $V_o$  are considered constant, respectively. The transformer Thus the magnetizing inductor  $L_m$  and leakage inductor  $L_{lk}$  with the turns ratio of 1: N,

where  $N = \frac{N_s}{N_p}$ .  $L_{lk}$  is assumed to be much smaller than  $L_m$ .

The capacitor  $C_r$  is the resonant capacitor.  $C_r$  resonates with the leakage inductor  $L_{lk}$ . Thus, the resonant capacitor voltage  $V_r$  is not considered constant for one switching period. Fig.2. shows the switching waveforms of the proposed converter during one switching period  $T_s (= \frac{1}{f_s})$ .

Fig.2. (a) shows the switching waveforms at the primary side. Fig.2. (b) shows the switching waveforms at the secondary side. The proposed converter has six switching modes during  $T_s$ . The duty ratio  $D$  is based on the on-time of the main switches. Fig. 3 shows the switching modes of the proposed converter during  $T_s$ . Before  $t = t_0$ ,  $S_2$  and  $S_3$  have been turned OFF. The voltages  $V_{s1}$  and  $V_{s4}$  have been zero when the primary current  $i_p$  flows through the body diodes  $D_{s1}$  and  $D_{s4}$ .

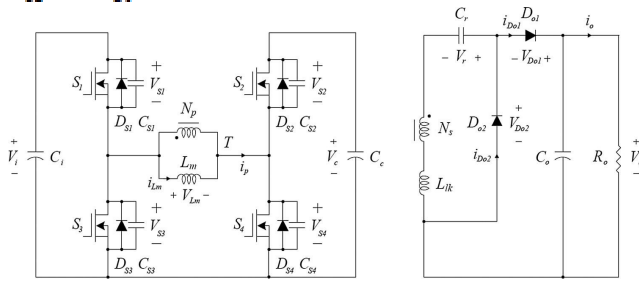
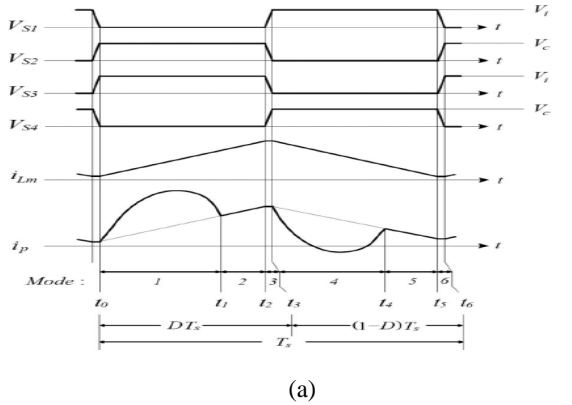
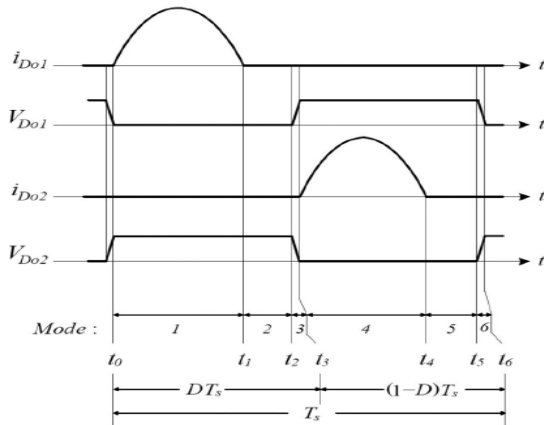


Fig.1.Circuit diagram of the proposed converter



(a)



(b)

Fig.2. Switching wave forms of the proposed converter during  $T_s$ : (a) Waveforms at the primary side and (b) Waveforms at the secondary side.

The proposed converter has six distinct operating modes for  $T_s$  as follows:

**Mode 1 [ $t_0, t_1$ ]:** At  $t = t_0$ , and  $S_4$  are turned ON. Since  $V_{Lm} = V_i$ , the magnetizing inductor current  $i_{Lm}$  increases linearly as

$$i_{Lm}(t) = i_{Lm}(t_0) + \frac{V_i}{L_m}(t - t_0) \quad (1)$$

At the secondary side,  $NV_i$  is applied to the secondary winding of  $T$ . The output diode  $D_{o1}$  is turned ON. The series-resonant circuit consisting of  $L_{lk}$  and  $C_r$  is formed. By the series resonance between  $L_{lk}$  and  $C_r$ , the energy stored in  $C_r$  is transferred to  $C_o$ . The angular resonant frequency  $\omega_r$  of the series-resonant circuit is

$$\omega_r = 2\pi f_r = \frac{1}{\sqrt{L_{lk} C_r}} \quad (2)$$

Where  $f_r$  is the resonant frequency. By referring the output diode current  $i_{Do1}$  to the primary side, the primary current  $i_p$  is expressed as

$$i_p(t) = i_p(t_0) + \frac{V_i}{L_m}(t - t_0) + N i_{Do1}(t) \quad (3)$$

Where the output diode current  $i_{Do1}$  is given by

$$i_{Do1}(t) = \frac{V_o - NV_i - V_r}{Z_r} \sin \omega_r(t - t_0) \quad (4)$$

The resonant impedance  $Z_r$  is expressed as

$$Z_r = \sqrt{\frac{L_{lk}}{C_r}} \quad (5)$$

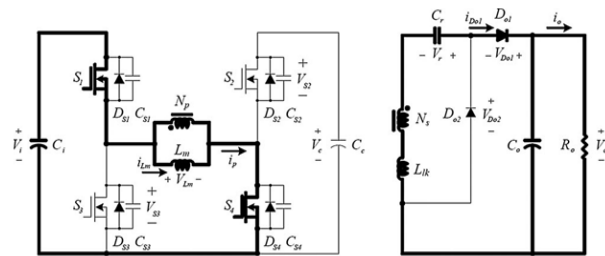


Fig.3(a): Mode 1

**Mode 2 [ $t_1, t_2$ ]:** At  $t = t_1$ , the half-resonant period of the series resonance is finished. The output diode current  $i_{Do1}$  is zero before  $D_{o1}$  is turned OFF.  $D_{o1}$  can be turned off at zero current without any diode reverse recovery current at the end of Mode2.

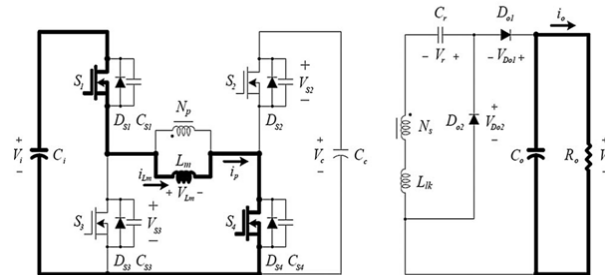


Fig.3(b): Mode 2

**Mode 3** [ $t_2, t_3$ ]: At  $t = t_2$ ,  $S_1$  and  $S_4$  are turned OFF. The primary current  $i_p$  charges  $C_{s1}$  and  $C_{s4}$  and discharges  $C_{s2}$  and  $C_{s3}$ .  $V_{s1}$  and  $V_{s4}$  increase from zero to  $V_i$ .  $V_{s2}$  and  $V_{s3}$  decrease from  $V_c$  to zero. Since the switch output capacitor  $C_s (= C_{s1} = C_{s2} = C_{s3} = C_{s4})$  is very small, the time interval during this mode is considered negligible compared to  $T_s$ .

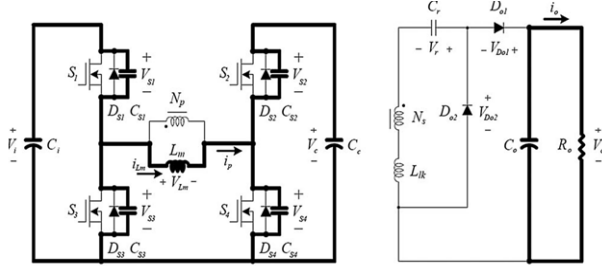


Fig.3(c):Mode 3

**Mode 4** [ $t_3, t_4$ ]: At  $t = t_3$ , and  $S_2$  are turned ON. Since  $V_{Lm} = -V_c$ , the magnetizing inductor current  $i_{Lm}$  decreases linearly as

$$i_{Lm}(t) = i_{Lm}(t_3) - \frac{V_c}{L_m}(t - t_3) \quad (6)$$

At the secondary side,  $NV_c$  is reversely applied across the secondary winding of  $T$ . The output diode  $D_{o2}$  is turned ON. The series-resonant circuit consisting of  $L_{rk}$  and  $C_r$  is formed again. The input power is transferred to  $C_r$  by the series resonance between  $L_{rk}$  and  $C_r$ . By referring the output diode current  $i_{D_{o2}}$  to the primary side, the primary current  $i_p$  is expressed as

$$i_p(t) = i_p(t_3) - \frac{V_c}{L_m}(t - t_3) - N i_{D_{o2}}(t) \quad (7)$$

Where the output diode current  $i_{D_{o2}}$  is given by

$$i_{Lm}(t) = i_{Lm}(t_3) - \frac{N V_c + V_r}{Z_r} \sin \omega_r (t - t_3) \quad (8)$$

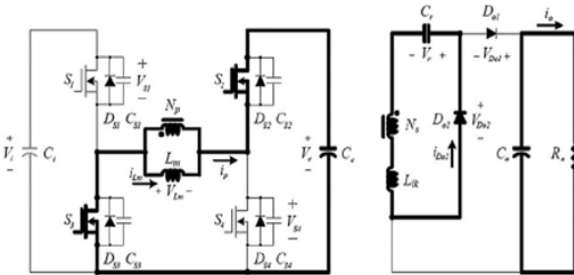


Fig.3(d):Mode 4

**Mode5** [ $t_4, t_5$ ]: At  $t = t_4$ , the half-resonant period of the series resonance is finished. The output diode current  $i_{D_{o2}}$  is zero before  $D_{o2}$  is turned OFF.  $D_{o2}$  can be turned OFF without any diode reverse-recovery current.

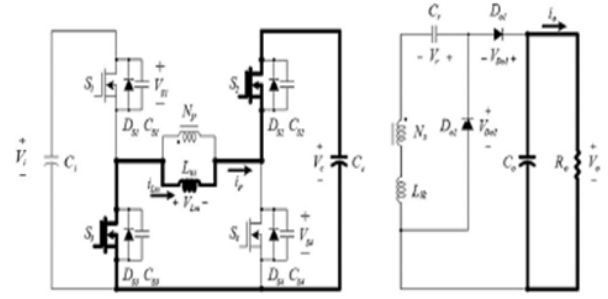


Fig.3(e):Mode 5

**Mode 6** [ $t_5, t_6$ ]: At  $t = t_5$ ,  $S_2$  and  $S_3$  are turned OFF. The primary current  $i_p$  charges  $C_{s1}$  and  $C_{s2}$  and discharges  $C_{s3}$  and  $C_{s4}$ .  $V_{s2}$  and  $V_{s3}$  increase from zero to  $V_c$ .  $V_{s1}$  and  $V_{s4}$  decrease from  $V_i$  to zero. Since the capacitor  $C_s$  is very small, the time interval during this mode is considered negligible compared to  $T_s$ . The next switching cycle begins when  $S_1$  and  $S_4$  are turned ON again.

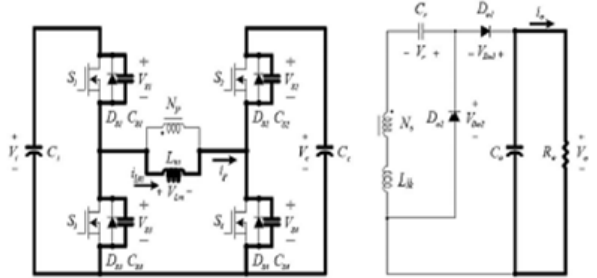


Fig.3(f):Mode 6

By the voltage-second balance relation on the magnetizing inductor  $L_m$ , the voltages  $V_c$  and  $V_r$  are expressed as

$$V_c = \frac{D}{1-D} V_i \quad (9)$$

$$V_r = (1-D) V_c \quad (10)$$

For the voltage-second balance relation on the secondary winding of  $T$  during  $T_s$ , the following relation between the output voltage  $V_o$  and the input voltage  $V_i$  is obtained as

$$\frac{V_o}{V_i} = \frac{N}{1-D} \quad (11)$$

The maximum voltage stress of  $s_1$  and  $s_3$  is confined to the input voltage  $V_i$ . The voltage stress of  $s_2$  and  $s_4$  is confined to the clamping capacitor voltage  $V_c$ . The clamping capacitor voltage in case of the dual active-clamping circuit is always lower than the clamping capacitor voltage in case of the conventional active-clamping circuit. It means that the switch voltage stress of the proposed converter is always lower than the switch voltage stress of the previous converter using the conventional active-clamping circuit. Especially, when the duty ratio is below 0.5, the clamping capacitor voltage can be lower than the input voltage  $V_i$ . It is critically beneficial in low-voltage PV applications where more than 50% of the power losses are lost as switching power losses. The output diode currents  $i_{D_{o1}}$  and

$iD_{02}$  should be zero before the output diodes  $D_{01}$  and  $D_{02}$  are turned OFF. The half-resonant period of the series resonance during Mode 1 and Mode 4 should be finished before the output diode is turned OFF. The following condition should be satisfied for zero-current turn-off of the output diode as

$$\sin[\omega_c D_{max} T_s] = 0, \quad \text{if } D_{max} \leq 0.5 \quad (12)$$

$$\sin[\omega_c (1 - D_{max}) T_s] = 0, \quad \text{if } D_{max} > 0.5 \quad (13)$$

Where  $D_{max}$  is the maximum duty ratio.  $\omega_c$  is the critical angular resonant frequency as  $\omega_c = 2\pi f_c$ .  $f_c$  is the critical resonant frequency of the series-resonant circuit. For zero-current turnoff of the output diode, the resonant frequency  $f_r$  should be higher than the critical resonant frequency  $f_c$ . Then, the resonant capacitor  $C_r$  should be determined as

$$C_r < \frac{1}{\omega_c^2 L_{lk}} = \frac{D_{max}^2 T_s^2}{\pi^2 L_{lk}}, \quad \text{if } D_{max} \leq 0.5 \quad (14)$$

$$= \frac{(1 - D_{max})^2 T_s^2}{\pi^2 L_{lk}}, \quad \text{if } D_{max} > 0.5 \quad (15)$$

### III. CONTROL STRATEGY

#### Fast Output Voltage Control

The output voltage  $V_o$  is controlled with the duty ratio  $D$ . When  $S_1$  and  $S_4$  are turned ON (Mode 1 and Mode 2), the magnetizing current  $iL_m$  increases linearly. The input energy is stored in the magnetizing inductor  $L_m$ . The following voltage relation is obtained as

$$V_i - L_m \frac{di_{Lm}}{dt} \quad (16)$$

When  $S_2$  and  $S_3$  are turned ON (Mode 4 and Mode 5), the magnetizing current decreases  $iL_m$  linearly. The energy stored in  $L_m$  is transferred to  $C_c$ . The following voltage relation is obtained:

$$V_i - L_m \frac{di_{Lm}}{dt} - V_c = 0 \quad (17)$$

From (16) and (17), depending on the duty ratio  $D$  of the switches, the average magnetizing inductor voltage during  $T_s$  gives the following relation:

$$V_i D T_s + (V_i - V_c)(1 - D) T_s = L_m \Delta i_{Lm} \quad (18)$$

where  $\Delta i_{Lm}$  is the ripple current of the magnetizing inductor during  $T_s$ . By using (9) and (11), (18) can be written as

$$V_i D + \left(V_i - \frac{V_c}{N}\right)(1 - D) = L_m \frac{\Delta i_{Lm}}{T_s} \quad (19)$$

Then, the duty ratio  $D$  is represented by

$$D = D_n + D_c \quad (20)$$

Where  $D_n$  is a nominal duty ratio and  $D_c$  is a controlled duty ratio. The nominal duty ratio  $D_n$  and the controlled duty ratio  $D_c$  can be, respectively, represented as

$$D_n = 1 - \frac{NV_i}{V_c} \quad (21)$$

$$D_c = \frac{NL_m \Delta i_{Lm}}{V_c T_s} \quad (22)$$

Then, the duty ratio  $D$  becomes

$$D = D_n + D_c = 1 - \frac{NV_i}{V_c} + \frac{NL_m \Delta i_{Lm}}{V_c T_s} \quad (23)$$

To regulate the output voltage for the output load variation, the conventional PI controller can be used for the controlled duty ratio  $D_c$  as

$$D_c = K_p e + K_i \int e dt \quad (24)$$

$$e = V_o^* - V_o \quad (25)$$

Where  $V_o^*$  is the reference output voltage,  $e$  is the voltage error between  $V_o^*$  and  $V_o$ , and  $K_p$  and  $K_i$  are the PI control gains of the controller, respectively. The regulated output voltage is an important factor achieving high performance. The PV MIC system should provide a fast dynamic response for the grid power demand in case of the distributed generation using the renewable energy sources [1]. When the local load power increases or decreases abruptly, the output voltage of the dc-dc converter fluctuates as the inverter load changes. It might cause grid current harmonic distortion, damaging the grid connected power generation systems [7]. However, because the conventional PI controller controls the output voltage slowly, the output voltage variation exists. To reduce the output voltage variation, a modified PI controller is suggested. The suggested controller is

$$D_c = K_p e_m + K_i \int e_m dt \quad (26)$$

$$e_m = (V_o^* - V_o) \times \left(1 + \frac{|V_o^* - V_o|}{\alpha}\right) \quad (27)$$

Where  $e_m$  is the modified error between  $V_o^*$  and  $V_o$ .  $\alpha$  is the scaling factor. Compared to the error term of the conventional PI controller, the term  $|V_o^* - V_o| / \alpha$  is included. Due to the term  $|V_o^* - V_o| / \alpha$ , a large error between  $V_o^*$  and  $V_o$  increases  $e_m$  more than  $e$ . Thus, if the voltage error is large, the output voltage can be rapidly controlled as the suggested controller has a large gain. In contrast, if the voltage error is small, the suggested controller gives almost the same characteristic as the conventional PI controller.

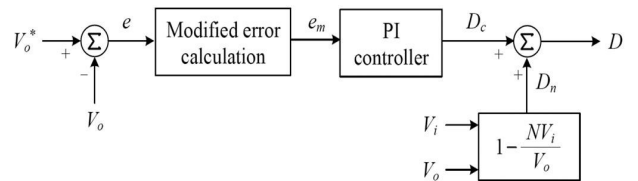


Fig.4. Control block diagram of the output voltage controller

### IV. RESULTS AND DISCUSSION

The proposed DC-DC converter with dual active-clamping circuit for low voltage PV sources is simulated in MATLAB-SIMULINK.

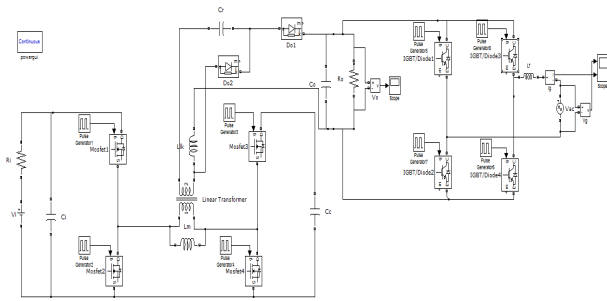
The values of the circuit parameters are given below:

- 1) Input voltage,  $V_i$ : 50 V;
- 2) Output voltage,  $V_o$ : 350 V;
- 3) Output power,  $P_o$ : 200 W;
- 4) Switching frequency,  $f_s$ : 50 kHz;
- 5) input capacitor,  $C_i$ : 13.2 mF;
- 6) Clamping capacitor,  $C_c$ : 680  $\mu$ F;
- 7) switch output capacitor,  $C_s$ : 500 pF;
- 8) Transformer turns ratio,  $N$ : 4;

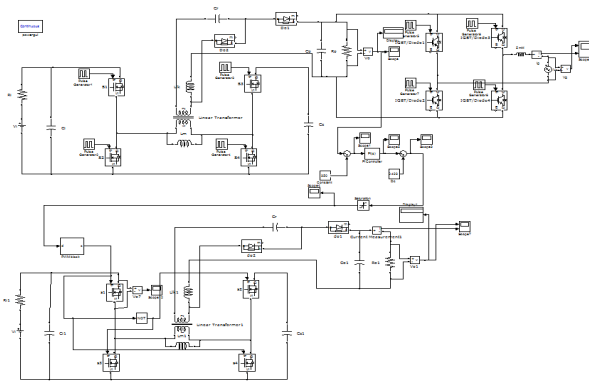
- 9) Magnetizing inductor,  $L_m$ :  $9 \mu\text{H}$ ;
- 10) Leakage inductor,  $L_k$ :  $3 \mu\text{H}$ ;
- 11) Resonant capacitor,  $C_r$ :  $0.4 \mu\text{F}$ ;
- 12) Output capacitor,  $C_o$ :  $220 \mu\text{F}$ .

Fig. 5 shows the Simulink models of the proposed converter with and without pi controller. Fig. 6 shows the primary current  $i_p$  and switch voltages  $V_{S1}$  and  $V_{S3}$  for 200 W output power. Fig. 6 shows the simulation waveforms at 50 V input voltage. As shown in Figs. 6,  $V_{S1}$  and  $V_{S3}$  are clamped at the input voltage. Fig. 7 shows the clamping capacitor voltage  $V_c$ , and switch voltages  $V_{S2}$  and  $V_{S4}$  for 200 W output power. Fig. 7 shows the simulation waveforms at 50 V input voltage. The clamping capacitor voltage  $V_c$  is 48 V.  $V_{S2}$  and  $V_{S4}$  are clamped at 48 V. Fig. 8 shows output diode voltage  $V_{D1}$ , output diode voltage  $V_{D2}$ , output diode current  $i_{D1}$ , output diode current  $i_{D2}$ . Fig. 9 shows experimental results for 50-V input voltage, output load voltage  $V_o$ , output load current  $i_o$ .

Fig. 10 shows the measured power efficiencies of the converters at 50 V input voltage for different output load conditions. The proposed converter achieves the efficiency of 97.5 % for 200 W output power. The previous active-clamped converter achieves the efficiency of 97.2 % for 200 W output power. The efficiency of 0.3% is improved by the proposed converter at 50 V input voltage for 200 W output power. The previous half-bridge converter achieves the efficiency of 97.0 % for 200 W output power. The proposed converter achieves the highest efficiency for the rated output power. Switching power losses are reduced by decreasing the voltage stress of power switches in the proposed converter. The power efficiency is increased by reducing switching power losses.



(a)



(b)

Fig. 5. Simulation models of Proposed DC-DC converter with dual active-clamping circuit. (a) Without PI controller (b). With PI controller. Waveforms at 50-V input voltage for 200-W output power.

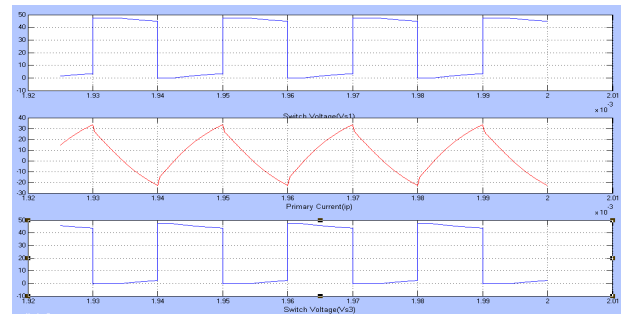


Fig. 6. Experimental results: primary current  $i_p$ : 10A/division; switch voltage  $V_{S1}$ : 10V/division; switch voltage  $V_{S3}$ : 10V/division.

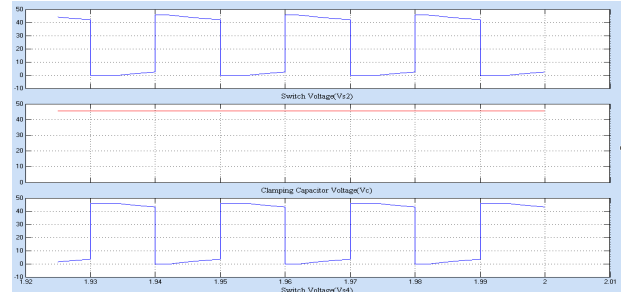


Fig. 7. Experimental results: Switch voltage  $V_{S2}$ : 10V/division; switch voltage  $V_{S4}$ : 10V/division; Clamping capacitor  $V_c$ : 10V/division, 10μs/division.

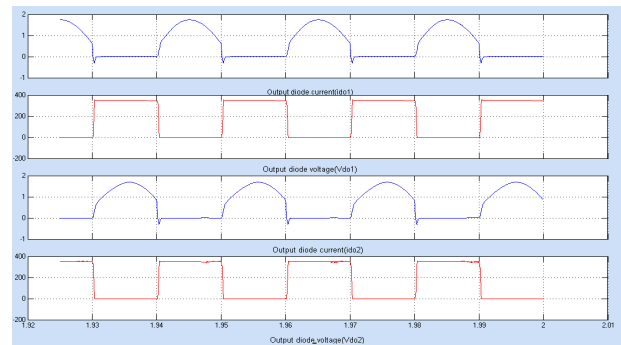
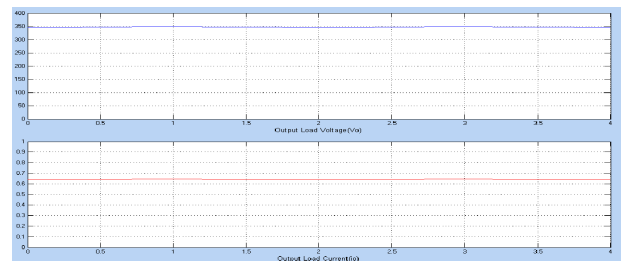


Fig. 8. Experimental results: Output diode voltage  $V_{D1}$ : 100V/Division; Output diode voltage  $V_{D2}$ : 100V/ division; Output diode current  $i_{D1}$ : 0.5A/division; Output diode current  $i_{D2}$ : 0.5A/division, 10μs/division.





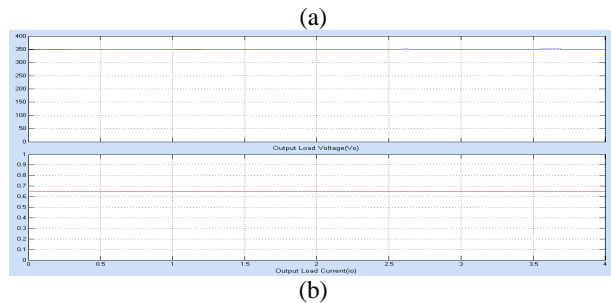


Fig.9.Experimental results: Output load voltage  $V_o$ : 100V/division; output load current 0.1A/division, 5 $\mu$ s/division: (a)in case of without using PI controller;(b) in case of with PI controller.

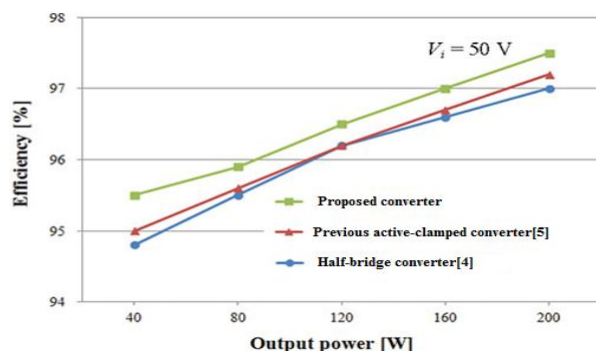


Fig.10. Experimental results: measured efficiency of the proposed converter compared with the efficiency of the previous converter.

## V. CONCLUSION

This paper has proposed a DC–DC converter with dual active-clamping circuit for low-voltage PV sources. The operation of the proposed converter has been described. The control strategy has been presented, including the fast output voltage control and its digital implementation. The proposed converter reduces the switching power losses, increasing power efficiency. The modified PI controller has been suggested for fast output voltage control. The proposed converter has the following

Advantages:

- 1) High efficiency and high-voltage conversion ratio;
- 2) Low switching losses by reduced voltage stress of power Switches;
- 3) Fast output voltage regulation for output load variation.

The proposed controller has been easily implemented by using a single-chip microcontroller. The performance of the proposed converter has been verified based on an experimental prototype for a 200-W PV module. The proposed converter achieves a high-efficiency of 97.5% at 50-V input voltage for 200-W output power.

## REFERENCES

- [1] L. Zhang, K. Sun, Y. Xing, L. Feng, and H. Ge, "A modular grid-connected photovoltaic generation system based on DC bus," *IEEE Trans. Power Electron.*, vol. 26, no. 2, pp. 523–531, Feb. 2011.

- [2] M. Cacciato, A. Consoli, R. Attanasio, and F. Gennaro, "Soft-switching converter with HF transformer for grid-connected photovoltaic systems," *IEEE Trans. Ind. Electron.*, vol. 57, no. 5, pp. 1678–1686, May 2010.

- [3] S. Bin and L. Zhengyu, "An interleaved totem-pole boost bridgeless rectifier with reduced reverse-recovery problems for power factor correction," *IEEE Trans. Power Electron.*, vol. 25, no. 6, pp. 1406–1415, Jun. 2010.

- [4] Z. Liang, R. Guo, J. Li, and A. Q. Huang, "A high-efficiency PV module integrated DC/DC converter for PV energy harvest in FREEDM systems," *IEEE Trans. Power Electron.*, vol. 26, no. 3, pp. 897–909, Mar. 2011.

- [5] W. Y. Choi, J. S. Yoo, and J. Y. Choi, "High efficiency dc–dc converter with high step-up gain for low PV voltage sources," in *Proc. IEEE ECCE Asia*, Jeju, Korea, May 30/Jun. 3, 2011, pp. 1161–1163.

- [6] M. Barai, S. Sengupta, and J. Biswas, "Digital controller for DVS-enabled dc–dc converter," *IEEE Trans. Power Electron.*, vol. 25, no. 3, pp. 557–573, Mar. 2010.

- [7] S. Kai, Z. Li, X. Yan, and J. M. Guerrero, "A distributed control strategy based on DC bus signaling for modular photovoltaic generation systems with battery energy storage," *IEEE Trans. Power Electron.*, vol. 26, no. 10, pp. 3032–3045, Oct. 2011.



**B.GAMYA** received B.Tech degree in Electrical and Electronic Engineering from Jawaharlal Nehru Technological University, Anaparthi, India in 2012. Currently She is pursuing M.Tech, Power Electronics in Sreenivasa Institute of Technology and Management Studies, Chittoor, A.P, India. Her research interests are development in Power Electronics.



**RAMESH R. HALAKURKI** Currently working as Professor in department of Electrical and Electronics Engineering, Sreenivasa Institute of Technology and Management Studies, Chittoor, A.P, India. His research interests include Power Electronics and Neural networks. He is a life member of ISTE, Associate Member of IE.